Synthetic aperture tomographic phase microscopy for 3D imaging of live cells in translational motion

Niyom Lue[1], Wonshik Choi[1,*], Gabriel Popescu[2], Kamran Badizadegan[1,3], Ramachandra R. Dasari[1], and Michael S. Feld[1]

[1]*G. R. Harrison Spectroscopy Laboratory, Massachusetts Institute of Technology, Cambridge, Massachusetts 02139, USA*
[2]*Department of Electrical and Computer Engineering, University of Illinois at Urbana-Champaign, Illinois 61801, USA*
[3]*Department of Pathology, Harvard Medical School and Massachusetts General Hospital, Massachusetts 02114, USA*
[*]*Corresponding author: wonshik@mit.edu.*

Abstract: We present a technique for 3D imaging of live cells in translational motion without need of axial scanning of objective lens. A set of transmitted electric field images of cells at successive points of transverse translation is taken with a focused beam illumination. Based on Hyugens' principle, angular plane waves are synthesized from E-field images of a focused beam. For a set of synthesized angular plane waves, we apply a filtered back-projection algorithm and obtain 3D maps of refractive index of live cells. This technique, which we refer to as synthetic aperture tomographic phase microscopy, can potentially be combined with flow cytometry or microfluidic devices, and will enable high throughput acquisition of quantitative refractive index data from large numbers of cells.

©2008 Optical Society of America

OCIS codes: (120.3180) Interferometry; (180.0180) Microscopy; (170.3880) Medical and biological imaging.

References and links

1. B. E. Bouma and G. J. Tearney, *Handbook of optical coherent tomography* (2001).
2. W. Tan, A. L. Oldenburg, J. J. Norman, T. A. Desai, and S. A. Boppart, "Optical coherence tomography of cell dynamics in three-dimensional tissue models," Opt. Express **14**, 7159-7171 (2006).
3. J. B. Pawley, *Handbook of biological confocal microscopy* (2006).
4. M. Slaney and A. C. Kak, "Diffraction tomography," Proc. Soc. Photo. Opt. Instrum. Eng. **413**, 2-19 (1983).
5. W. Choi, C. Fang-Yen, K. Badizadegan, S. Oh, N. Lue, R. R. Dasari, and M. S. Feld, "Tomographic phase microscopy," Nature Methods **4**, 717-719 (2007).
6. G. G. Levin, G. N. Vishnyakov, C. S. Zakarian, A. V. Likhachov, V. V. Pickalov, G. I. Kozinets, J. K. Novoderzhkina, and E. A. Streletskaya, "Three-dimensional limited-angle microtomography of blood cells: experimental results," Proc. SPIE **3261**, 159-164 (1998).
7. F. Charriere, A. Marian, F. Montfort, J. Kuehn, T. Colomb, E. Cuche, P. Marquet, and C. Depeursinge, "Cell refractive index tomography by digital holographic microscopy," Opt. Lett. **31**, 178-180 (2006).
8. V. Lauer, "New approach to optical diffraction tomography yielding a vector equation of diffraction tomography and a novel tomographic microscope," J. Microsc. **205**, 165-176 (2002).
9. M. Zysk, J. J. Reynolds, D. L. Marks, P. S. Carney, and S. A. Boppart, "Projected index computed tomography," Opt. Lett. **28**, 701-703 (2003).
10. D. Nahamoo, S. X. Pan, and A. C. Kak, "Synthetic aperture diffraction tomography and its interpolation – free computer implementation," IEEE Trans. Sonics and Ultrason. **31**, 218-229 (1984).
11. T. S. Ralston , D. L. Marks, P. S. Carney, and S. A. Boppart, "Interferometric synthetic aperture microscopy," Nature Phys. **3**, 129-134 (2007).
12. N. Lue, W. Choi, G. Popescu, K. Badizadegan, R. R. Dasari, and M. S. Feld, "Confocal diffraction phase microscopy of live cells," Opt. Lett. **33**, 2074-2076 (2008).
13. N. Lue, G. Popescu, T. Ikeda, R. R. Dasari, K. Badizadegan, and M. S. Feld, Live cell refractometry using microfluidic devices, Opt. Lett. 31, 2579 (2006).

14. M. Born and E. Wolf, *Principles of optics* (1999).

15. C. Fang-Yen, S. Oh, Y. Park, W. Choi, S. Song, H. S. Seung, R. R. Dasari, and M. S. Feld, "Imaging voltage-dependent cell motions with heterodyne Mach-Zehnder phase microscopy," Opt. Lett. **32**, 1572-1574 (2007).

16. X. Zhong, "A four-frame phase shift method insensitive to phase shifter nonlinearity," J. Opt. A: Pure Appl. Opt. **8**, 300-303 (2006).

17. A. C. Kak and M. Slaney, *Principles of Computerized Tomographic Imaging* (1988).

1. Introduction

There have been several 3D imaging methods in optical microscopy which can visualize cellular and sub-cellular structures of biological cells. Scanning a focused beam is a straightforward method widely used in confocal fluorescence microscopy and optical coherence tomography [1, 2]. 3D images can be obtained from full-field images taken with scanning objective focus, and applying deconvolution algorithm based on the point spread function of the optical system [3]. Filtered back-projection algorithm also provides a way to reconstruct 3D structures of object from a set of angular images, which is widely used in X-ray computed tomography [4] and recently applied to the tomographic phase microscopy [5] and other previous works [6-9].

All of these approaches require for a sample to be stationary while acquiring images. In this work, we propose an approach in which 3D images can be acquired for a sample in translational motion. According to Huygens' principle, any directional plane wave can be created from a set of position-dependent focused beams. By measuring the phase and amplitude of a focused beam with a sample translating across the beam, plane waves with any incident directions can be synthesized. From a set of angular phase images of synthesized plane waves, a 3D image can be constructed using a filtered back projection algorithm. This source translation technique, referred to as synthetic aperture tomographic phase microscopy (sTPM), was first suggested by Nahamoo et al [10] for ultrasound imaging, but has never been before implemented in the optical regime. Another interesting technique, imaging synthetic aperture microscopy (ISAM) [11], synthesizes the signals from focused illumination in the reflection geometry to improve the axial resolution of Fourier domain optical coherence tomography. Although ISAM is being used for in-vivo study, it does not provide quantitative refractive index information.

Similar to the confocal microscopy, sTPM uses a focused beam as an illumination source, in a similar geometry to what we described in a recent report [12]. The previous work demonstrates 2D quantitative phase imaging using a focus line beam illumination. In the current study, we extend these measurements to 3D reconstructions, as a result sTPM can obtain 3D map of object without need of scanning objective along axial direction.

In this letter, we present the first optical implementation of synthetic aperture tomography to map the 3D distribution of refractive index in live cells when they are under translational motion. This technique can potentially be incorporated into flow cytometry and other microfluidic systems, and can thus enable rapid data acquisition for a large number of cells [13]. The ability to rapidly process cells in large numbers opens the possibility of clinical applications of early stage disease identification in which slight changes in a small number of differentiated cells are detected in the presence of a large number of normal cells.

2. Synthetic aperture tomography theory

According to Huygens' principle, every point on the wavefront of a propagating wave serves as the source of secondary spherical wavelets. Thus, any wavefront can be synthesized by a set of spherical waves. Experimentally, a tightly focused Gaussian beam can be approximated as a spherical wave. A set of focused fields can be used to generate a plane wave propagating in any direction. For 2-D object in the x-z plane with x-axis in the transverse plane and z in the axial plane, a focus beam can be represented as a weighted set of plane waves as follows:

$$E(x,z) = \int A(k_x)\exp(-ik_x x + ik_z z)\,dk_x, \tag{1}$$

where $A(k_x)$ is the complex amplitude of an individual plane wave with spatial frequency k_x. The wave number in the medium, $k_0 = 2\pi/\lambda'$ is fixed with $\lambda' = \lambda_0/n_{medium}$, the wavelength in the medium; k_z is determined by the relation $k_z = \left[k_0^2 - k_x^2\right]^{1/2}$. After interacting with a specimen, the transmitted field at the detector, located at $z = z'$, can be rewritten as a weighted sum of plane waves:

$$E(x,z') = \int A(k_x)\exp[-i\{k_x x + k_z z' + \phi(x;k_x)\}]\,dk_x, \tag{2}$$

where $\phi(x;k_x)$ is a complex phase induced by a sample for each plane wave component k_x. Since these plane waves are being combined through integration, each plane wave component cannot be algebraically solved. To detangle the effect of integration, source translation along an axis perpendicular to the propagation direction is introduced. From moving the source along x-direction by η, the translated plane wave can be decomposed as follows:

$$E(x;\eta,z') = E(x-\eta,z') = \int \left(A(k_x)\exp(ik_x\eta)\right)\exp[-i\{k_x x + k_z z' + \phi(x;k_x)\}]\,dk_x. \tag{3}$$

The additional phase term $\exp(ik_x\eta)$ is introduced as the source moves. Note that the phase shift of this additional term is dependent on k_x. As a result, Fourier Transform of $E(x;\eta,z')$ at particular η can be used to separate an individual spatial frequency component out of integration as follows:

$$\int E(x;\eta,z')e^{-ik_\eta \eta}\,d\eta = \int[\int \exp\{-i(k_\eta - k_x)\eta\}\,d\eta]\,A(k_x)\exp[-i\{k_x x + k_z z' + \phi(x;k_x)\}]\,dk_x,$$
$$= A(k_\eta)\exp[-i\{k_\eta x + (k_0^2 - k_\eta^2)^{1/2}z' + \phi(x;k_\eta)\}]. \tag{4}$$

The relationship, $\int \exp\{-i(k_\eta - k_x)\eta\}\,d\eta = \delta(k_\eta - k_x)$, eliminates the need of the integration over k_x and a complex phase $\phi(x;k_\eta)$ of each spatial frequency component k_η can be obtained. Since an individual plane wave is retrieved by Fourier transformation, the process can also be interpreted as a synthesis of focused beams with a translation-dependent additional phase factor, $\exp(-ik_\eta \eta)$. As a result, this method was referred to as synthetic aperture (SA) [10].

Using the relationship, $k_\eta = k_0 \sin\theta$, with θ the propagation direction of plane wave relative to the optic axis, the angular phase image, $\phi(x;\theta)$, can be determined. By interpreting the phase image as an integration of the refractive index along the beam propagation direction, a filtered back-projection algorithm can be used to obtain the 3-D map of refractive index [5-7].

3. Experimental setup

In sTPM, a cylindrical lens is used to focus the collimated beam to a line beam allowing single directional scan in a transverse plane. At the Fourier plane after cylindrical lens, one axis is a focused beam while the other axis is a plane wave. To simplify nomenclature, the axis along the focused beam direction is named a Fourier axis and the other is named an Imaging axis. In this configuration, the reconstruction problem is also reduced to 2D instead of 3D since the Imaging axis can be treated independently.

To utilize the synthetic aperture algorithm, both phase and amplitude of the transmitted E-field have to be recorded. Interferometry is widely used to measure the E-field [14]; however a coherent plane wave is typically used as a illumination to generate uniform contrast of

interference across the field of view. For a focused beam, limited dynamic range of detector impedes the proper recording of the large intensity variation. To reduce spatial intensity variation of the focused beam, a cylindrical lens is installed after the image plane to carry out optical Fourier transform along the Fourier axis. The optical transformation of the high spatial variation of the focused beam gives the uniform intensity distribution, which is ideally for recording. By numerical process with inverse Fourier transform to the recorded image, the E-field image of the line focus beam at the image plane can be obtained from the numerical Fourier transform of the recorded image along the Fourier axis.
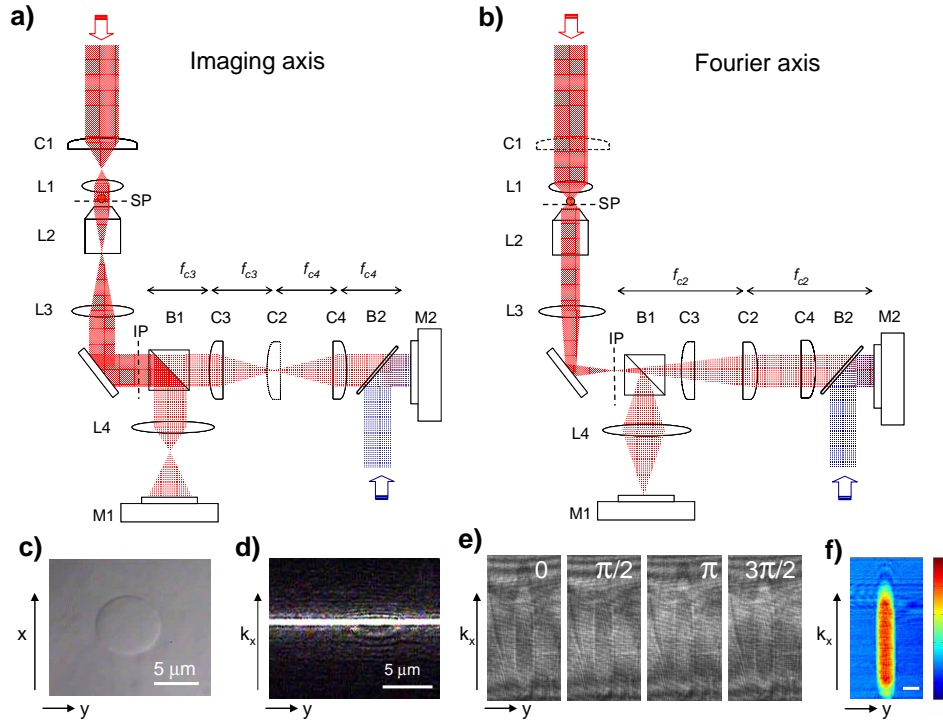

Fig 1. Experimental setup. Two views depend on the axes of cylindrical lenses are shown: (a) Imaging axis in which the illumination beam is a plane wave, (b) Fourier axis in which the illumination is a focused beam. C1-4 are cylindrical lenses with focal lengths 10, 20, 40 and 20 cm. L1 is a 1.4 NA condenser lens (Nikon). L2 is a 100x objective lens (Zeiss). L3 a tube lens, and L4 is the image lens with focal length of 20 cm. B1 and B2 are beam splitters. M1 is the CCD camera (Fastcam 1024PCI, Photron) and M2 is the video camera (TC-84, Sony). (c) Bright field image of a 10 µm polystyrene bead. (d) Line focus beam through a bead imaged at camera M1. (e) Four consecutive $\pi/2$ phase-shifted interferometric images of the bead imaged at camera M2. (f) Quantitative phase image of the bead processed from (e).

Another modification is made to sTPM solely to be more applicable to flow. Instead of scanning the illumination beam along the Fourier axis as introduced in theory, the sample is translated across the line focused beam. The relative position of the sample with respect to the illumination beam is then used for numerical processing.

The detailed experimental setup is shown in Fig.1. The E-field measurement is based on a heterodyne Mach-Zehnder interferometer [15]. The output of a HeNe laser (20 mw, $\lambda = 632.8$ nm from Melles Griot, USA) is split by an optical beam splitter (not shown). One beam (the object beam, shown in red) travels through the object located on the sample stage of an inverted microscope (Axiovert S100, Zeiss Germany). The other beam (reference beam, shown in blue) travels outside of the microscope, with its frequency shifted by a pair of acousto-optic modulators (not shown) to modulate the relative phase between the object and

the reference in time (see [10]). The focused beam at the sample is produced by a 4F configuration of a cylindrical lens (C1) and a high NA condenser (L1) lens (1.4 NA oil immersion, Nikon Japan). With the use of the cylindrical lens, the optical system is presented in two orthogonal axes: Imaging and Fourier axes. Planar axis (Figure 1(a)) has a plane wave illuminating beam at the sample and Fourier axis (Figure 1(b)) has a focused illuminating beam. The transmitted beam, which now is shaped as a line focus beam is magnified by an objective (L2; 100x oil immersion, Zeiss Germany,) and tube lens (L3), and relayed to the image plane (IP) at microscope's output port. A beam splitter (B1) is placed right after IP. The reflected beam containing the image is relayed to the video camera (M1; TC-87, Sony Japan) via a lens (L4). Figure 1(c) is a typical bright field image of a 10 μm polystyrene bead measured at M1. Note that a broadband LED (not shown) is used as a source and C1 is temporarily taken out. Figure 1(d) shows the line-focused beam illuminating the center of the same bead in (c), with the C1 in position.

The transmitted beam from B1 and the reference beam interfere to give the phase and amplitude of the field at the image plane. Note that the variation of intensity in line focus beam cannot simply be digitized by a CCD detector due to limited dynamic range. The focused beam is expanded in the Fourier axis by Fourier transforming with a cylindrical lens (C2). Simultaneously two cylindrical lenses C3 and C4 relay the image on the Imaging axis. This makes the Fourier axis in spatial frequency coordinate (k_x) and the Imaging axis in spatial coordinate (y) at the camera plane. The reference beam, a planar beam whose frequency is shifted by 1.25kHz using two acousto-optic modulators as mentioned previously [5,15] is brought to interfere with the expanded focused beam at a fast CMOS camera (M2; Fastcam 1024PCI, Photron Japan). The camera records four interferometric images at 5kHz frame rate. Typical interferogram images are shown in Fig. 1(e), when line focus beam is positioned about the center of a 10 μm bead. By applying a four-frame phase shifting interferometry (4f-PSI) algorithm [16], the phase image $\phi(k_x, y)$ is obtained (Fig. 1(f)). To generate a scanning point source for this synthetic aperture tomography, the sample is translated across the line focus beam, along the Fourier axis by a precision micro-position translation stage (PI M-216, Physik Instrumente Germany) with a step size of 0.1 μm.

4. Data acquisition and processing

A live HeLa cell (a primary cell line: cervical cancer cell) is imaged with sTPM. The cell was dissociated from culture dishes and incubated for 4 to 5 hours in a glass chamber to allow it attaching to glass substrate. A set of phase images, $\phi(k_x, y; \eta)$, taken as a function of sample translation η is shown in Fig. 2(a). The translation range is typically greater than twice the diameter of the sample. Corresponding amplitude images, $A(k_x, y; \eta)$, can also be obtained from the 4f-PSI algorithm. After combining both amplitude and phase to obtain the electric field, $E(k_x, y; \eta) = Ae^{i\phi}$, a numerical inverse Fourier transform is carried out along the k_x-axis to obtain $E(x; \eta, y)$. Figure 2(b) shows the resulting amplitude image in logarithmic scale. The illumination beam is stationary in the experiment and the sample is moving. In order to employ the synthetic aperture method, the sample is set to be stationary while the illumination beam is translated. Using known translation η from the translation stage, we numerically shift the image in the opposite direction of translation, which is equivalent to shifting the focused beam along x-direction while the sample is stationary.

With a set of E-field images $E(x; \eta, y)$ taken for the sample in translational motion, we applied synthetic aperture algorithm described in the theory section. For any given y, we take Fourier transform of $E(x; \eta, y)$ for the sample translation η as described in Eq. (4) as follows:

$$\tilde{E}(x; k_\eta, y, z') = \int E(x; \eta, y, z') \exp(-ik_\eta \eta)\, d\eta = A(k_\eta) \exp\left[-i\left\{k_\eta x + \sqrt{k_0^2 - k_\eta^2}\, z' + \phi(x, y; k_\eta)\right\}\right].$$

(5)

Dividing by the similar processed images taken without the sample, the phase image $\varphi(x, y; k_\eta)$ induced by the sample can be obtained (Fig. 2(c)). Using the relationship $k_\eta = k_0 \sin\theta$, with θ the direction of plane wave relative to the optic axis, the angular projection phase image, $\varphi(x, y; \theta)$, can be determined.
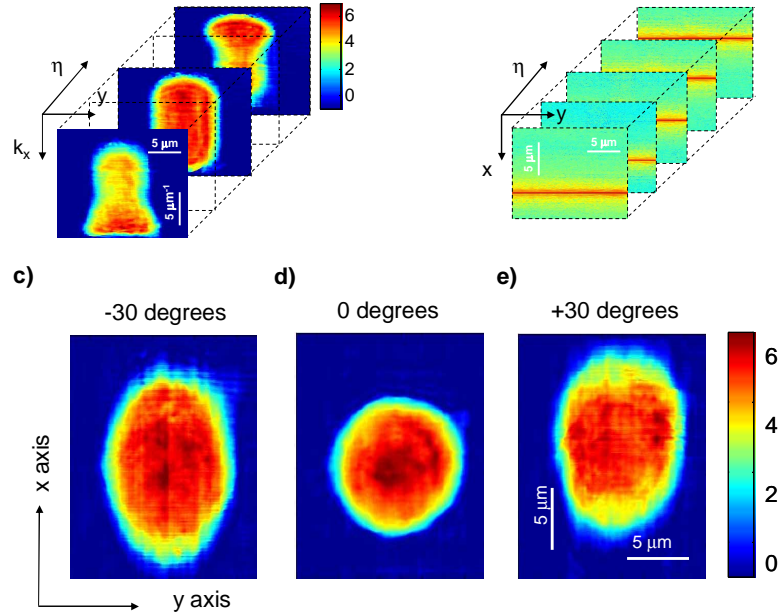

Fig. 2. Quantitative E-field images for a focused beam illumination. (a) Series of phase images while translating a HeLa cell. (b) Amplitude images at the image plane. (c-e) Synthesized quantitative phase images of a HeLa cell, equivalent to angular plane wave at -30°, 0° and +35°, respectively. Color bars indicate phase in radians.

Figures 2 (d-f) shows the phase image $\varphi(x, y; \theta)$ for a HeLa cell at angles (θ): -30, 0 and +30 degrees, respectively. Note that the phase image for nonzero degree is elongated along the tilting direction (x-axis). This is due to the fixed image plane during tilting illumination. A set of angular projection phase images ranging from -40 to 40 degrees can be synthesized from this system. After applying the filtered back-projection algorithm, the 3D map of refractive index is obtained by applying an inverse radon transform [17].
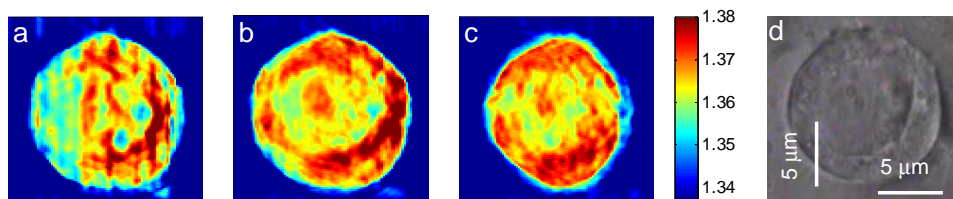

Fig. 3. Refractive index tomogram of a live HeLa cell. (a) – (c) Lateral slices of tomogram images for a HeLa cell in 2 µm steps from top to bottom. (d) Bright field image of the same HeLa cell. Color bar indicates refractive index at λ = 632.8 nm.

Figures 3(a)-(c) depict the x-y slices of the reconstructed tomogram of a HeLa cell with an axial distance of two microns between each slice image. Detailed structures such as nucleolus and nucleus are clearly visible, especially in Fig 3(b). A bright field image at approximately

same focus has been taken (Fig. 3(d)) to show the close correspondence with the tomogram. By using the refractive index of the culture medium, 1.337, measured in the previous study [8], the refractive index of the HeLa cell is found to be between 1.36-1.38. Similar to the result from tomographic phase microscopy [5], the heterogenous structures in cytoplasm have higher refractive index than the nucleus.

In this work, the angular range of the synthesized plane waves is narrower than our earlier work [5] which utilizes the direct illumination of plane waves with angles ranging from -60 to 60 degrees. The reason is due to the Gaussian intensity profile of the illumination, where the sensitivity of the signal detection is poor at large angles. As a result, the axial resolution is about 1 μm compared to previous 0.75 μm. Detectors with better dynamic range will improve the range of angle.

5. Summary and conclusions

Using synthetic aperture tomography, a novel quantitative tomographic phase microscopy technique, we have demonstrated the 3D imaging of live cells in translational motion. Although translation is controlled by a motorized stage in the present work, the method can be combined with flow cytometry or other translation/scanning methods, which makes it possible to continuously and rapidly image a large number of cells. We are aware of potential technical challenges in controlling flow. Non-uniform flow speed and cell motions other than translational could result in significant distortion in the 3D reconstruction process. Implementing laminar flow with precise control of the flow rate should help minimize these problems.

In future work, the data acquisition rate will be enhanced to enable detailed statistical analysis of the refractive index distribution of sub-cellular organelles. Given its quantitative and potentially high-throughput nature, synthetic aperture tomographic phase microscopy can potentially serve as a biomedical assay to differentiate or identify various cell populations, such as normal versus diseased cells.

Acknowledgments